

STUDY OF IRREGULAR ROUGHNESS IN MINIMAL CHANNELS

J. Yang¹, A. Stroh¹, S. Jakirlić², B. Frohnappel¹ and P. Forooghi^{3,*}

¹Institute of Fluid Mechanics, Karlsruhe Institute of Technology, Karlsruhe, Germany

²Institute of Fluid Mechanics & Aerodynamics, Technical University Darmstadt, Darmstadt, Germany

³Dept. Mechanical & Production Engineering, Aarhus University, Aarhus, Denmark

Abstract

Direct numerical simulation (DNS) is used to study turbulent flow over irregular rough surfaces in the periodic minimal channel configuration. The generation of irregular roughness is based on a mathematical random algorithm, in which the power spectrum (PS) of the roughness height function along with its probability density function (PDF) can be directly prescribed. In the present work both velocity field and temperature field are investigated. The hydro- and thermodynamic properties of the roughness, particularly the roughness function (ΔU^+) and the temperature profile offset ($\Delta\Theta^+$), are compared with those obtained from full span DNS for 6 roughness topographies with systematically varied PDF and PS configuration at $Re_\tau \approx 500$. The comparison confirms the capability of the minimal channel approach for characterization of irregular rough surfaces providing excellent agreement (within 5%) in ΔU^+ and $\Delta\Theta^+$ across various types of roughness topographies. Results also indicates that different random realizations of roughness, with a fixed PS and PDF, translate to similar prediction with a small scatter. Systematically varied PDF and PS show its impact to both ΔU^+ and $\Delta\Theta^+$. However It is reported that the effects of varying PDF and PS are different for skin friction and heat transfer.

1 Introduction

Rough surfaces are abundant in nature (e.g. river beds and complex terrain) and engineering (e.g. degraded turbine blades, fouled ship hulls and iced aircraft surfaces). It is well established that the topography of roughness can significantly affect its hydrodynamic properties. In practice, the most important hydrodynamic effect of roughness is an increase in the skin friction coefficient of the surface. This increase manifests itself in a downward shift in the logarithmic region of inner scaled mean velocity profile ΔU^+ , which is related to the equivalent sand-grain roughness k_s (Jiménez 2004). The latter parameter is widely used as an input to engineering applica-

tions. Therefore, the central importance of this mean velocity downward shift ΔU^+ in determining the hydrodynamic property of the roughness is understood, which is referred to as the (Hama) roughness function. To find ΔU^+ for an arbitrary roughness at a certain roughness flow regime, one needs to either run a laboratory (or high-fidelity numerical) experiment or use a so-called roughness correlation, which relates the topography of roughness to ΔU^+ . While the latter option is obviously less costly, large number of topographical metrics should be systematically investigated in constructing such a predictive correlation e.g. skewness $Sk(1/k_{rms}^3) \int_S (k - k_{md})^3 dS$ and $k_{rms} = \sqrt{(1/S) \int_S (k - k_{md})^2 dS}$ (Flack & Schultz 2010), effective slope $ES = (1/S) \int_S |\partial k / \partial x| dS$ (Napoli *et al.* 2008), roughness correlation length L_{corr} (Sigal & Danberg 2008).

Similar to the skin friction, roughness can enhance the heat transfer of the surface, designed roughness are often used in engineering applications (Forooghi *et al.* 2017a). However, it is widely understood that that the enhancement of heat transfer is not directly proportional to the increase of skin friction. This is reflected by the term 'Reynolds analogy factor' $RA = 2St/C_f$ (Bons 2005). Although, temperature profile of a forced convection smooth-wall flow is demonstrated also exhibits a logarithmic region (Kader 1981). The heat transfer of a rough wall can be also characterized by an analogous term to roughness function ΔU^+ , i.e. $\Delta\Theta^+$, where Θ represents the double-averaged temperature field. $\Delta\Theta^+$ describes the downward shift of the mean temperature logarithmic profile due to roughness relative to the smooth case with comparable Reynolds number Re_τ (Cebeci & Bradshaw 1984). Flack proposed use of Direct Numerical Simulation (DNS) for generating extensive data needed for a universal roughness correlation (Flack 2018). The major problems in reaching this goal are the computational cost of DNS and the measurements of realistic rough surfaces are rare and not suitable for systematic studies.

The aim of this work is to examine a new framework, which overcomes both obstacles. To

*Corresponding author's Email: forooghi@mpe.au.dk

relieve the computational cost we simulate the flow in fully developed turbulent channels with reduced streamwise and spanwise sizes. The idea was previously established and validated by Chung *et al.* (2015), MacDonald *et al.* (2016, 2019) with sinusoidal roughness structure. The criteria of the minimal channel size is given by the authors: $L_z^+ \geq \max(100, \tilde{k}^+/0.4, \lambda_{\sin}^+)$, $L_x^+ \geq \max(1000, 3L_z^+, \lambda_{\sin}^+)$. Where L_x and L_z are the streamwise and spanwise extend of the channel, respectively, \tilde{k} is the amplitude of the sinusoidal structure. λ_{\sin} represents the wavelength of the sinusoidal structure. The criteria are set with the aim of accommodating the minimal channel to the near wall turbulence as well as the roughness structure. The research shows that minimal channel following the criteria above is capable for this type of roughness (repetitive) structure to predict the roughness function ΔU^+ as well as the temperature offset $\Delta \Theta^+$, but has not been examined for irregular roughness up to now, i.e. the effect of repeating irregular roughness introduced by the significantly reduced size of minimal channel is yet unknown.

In order to evaluate the validity of this approach for irregular rough surfaces we employ the random algorithm proposed by Pérez-Ràfols & Almqvist (2019). With the roughness generation method surface is generated randomly while the roughness statistical properties can be controlled by its height probability density function (PDF) and the power spectrum (PS) (hence the term pseudo-random roughness). The generation process is realized by discrete fast fourier transform (DFFT), thus it is inherently suitable for the DNS simulations where periodic boundary condition is required.

In the present work, pseudo-random roughness with different prescription of PDF and PS are generated and simulated in both minimal channels and conventional full-span channels at $Re_\tau \approx 500$. The paper is organized in following way, in the roughness generation methodology along with the simulation setups will be illustrated. In simulation results from both minimal channels and full span channels are analyzed. Finally in conclusions are given.

2 Methodology

Pseudo-random roughness generation method

The pseudo-random roughness is generated with the method originally proposed by Pérez-Ràfols & Almqvist (2019), which will be referred to as generation method for the following text. The roughness structure function k is represented by discrete elevation map on 2-D Cartesian grid, i.e. $k(x, z)$, where x, z are the streamwise and

spanwise coordinate respectively. Initially, a roughness map with prescribed roughness PDF is given and is labeled as k_{PDF}^0 . This map do not necessarily contain desired PS. For the next step, this map is transformed using DFFT and compared with the second initial map with desired PS, which is labeled as k_{PS}^0 . After that, the field is transformed back with inverse DFFT and adjust the height distribution to fit the PDF. The iterative adjustment of PDF and PS continues until the error of PDF and PS, which are measured by the percentage disagreement of PDF and PS profile respectively, approaches a stationary low value. For further information readers are referred to the literature (Pérez-Ràfols & Almqvist 2019).

Direct numerical simulation

Direct numerical simulations are carried out in fully developed turbulent channels. Flow is driven by constant pressure gradient P_x . Periodic boundary condition is applied to the streamwise and spanwise boundaries of the channel. Upper and lower wall are roughened by the roughness structures. The roughness with no-slip & zero-temperature boundary condition is realized by imposing immersed boundary method (IBM) following Goldstein's method (Goldstein 1993). Where negative external force is applied to the flow in the roughness elements to obtain zero velocity & temperature inside the roughness. An source term $Q = \mathbf{u}$ is added to the temperature field to obtain a steady temperature field as the flow flowing through periodic channel and being cooled by the zero-temperature roughness boundaries. Thus, the Navier-Stokes equation writes:

$$\nabla \cdot \mathbf{u} = 0, \quad (1)$$

$$\frac{\partial \mathbf{u}}{\partial t} + \nabla \cdot (\mathbf{u} \mathbf{u}) = -\frac{1}{\rho} \nabla p + \nu \nabla^2 \mathbf{u} - \frac{1}{\rho} P_x \hat{\mathbf{e}_x} + \mathbf{F}_u, \quad (2)$$

$$\frac{\partial \theta}{\partial t} + \nabla \cdot (\mathbf{u} \theta) = \alpha \nabla^2 \theta + Q + \mathbf{F}_\theta, \quad (3)$$

where \mathbf{u} is the velocity vector $\mathbf{u} = (u, v, w)^\top$, P_x is the mean pressure gradient in the flow direction added as a constant and uniform source term to the momentum equation to drive the flow in the channel. Here p , $\hat{\mathbf{e}_x}$, ρ , ν , \mathbf{F}_θ and \mathbf{F}_u are pressure fluctuation, Kronecker delta, density, kinematic viscosity and external source term for momentum and energy equation due to IBM, respectively. The Friction Reynolds number is defined as $Re_\tau = u_\tau(H - k_{\text{md}})/\nu$, where $u_\tau = \sqrt{\tau_w}$ is the friction velocity and $\tau_w = -P_x(H - k_{\text{md}})$ is the wall shear stress controlled by the constant pressure gradient.

Description of cases

Thanks to the flexibility of the generation method, two of the roughness parameters cho-

sen from both PDF and PS sides are systematically varied and analyzed utilizing DNS, namely Sk and the PS slope p . Three values of Sk are selected i.e. $Sk \approx -0.48, 0, 0.48$. Skewed roughness distribution obeys Weibull's distribution, form factor is adjusted to match desired Sk , non-skewed roughness obeys the Gaussian distribution. Moreover the kurtosis $Ku \approx 3$ is selected for all roughness in search of the similarity to the Gaussian distribution. Therefore, the PDF are characterized in terms of negatively skewed, Gaussian and positively skewed distribution. The height of the roughness is scaled by the the 99% confidence interval of the PDF, which is denoted as k_{99} . $k_{99} = 0.1H$ is prescribed to all roughness configurations. In order to avoid extreme high/low roughness, roughness elements locate out side $1.2 \times k_{99}/2$ around the meltdown height $k_{md} = (1/S) \int_S k dS$ are excluded, where S is the wall-normal projection area of the surface.

On the other side, power-law PS is chosen, i.e. $E_k(\mathbf{q}) = C_0 (\|\mathbf{q}\| / q_0)^p$, where \mathbf{q} is the wavenumber vector $\mathbf{q} = (q_x, q_z)^\top$, $q_0 = 2\pi/\lambda_0$ is the referencing wavenumber corresponding to the largest in-plane length scale λ_0 , C_0 is a constant to scale the roughness height, and p is the slope of the power-law PS. p is chosen as -1 and -2 in seek of overlapping with previous researches (Barros *et al.* 2018, Nikora *et al.* (2019)). The cutoff wavelengths of the PS are selected to be moderate to the channel size as well as the grid resolution, i.e. the presenting roughness wavelength λ obeys $0.8H \leq \lambda \leq 0.08H$.

In summary, by "grid searching" of these two roughness parameters, in total 6 (3×2) roughness topographies are prescribed. Following abbreviation is used throughout the text to distinguish the cases:

$$\text{Topography} \quad \text{Channel size} \\ \underbrace{\boxed{G}}_{\text{PDF}} \quad \underbrace{\boxed{2}}_{-p} \quad | \quad \boxed{F} \quad . \quad (4)$$

- The first character indicates the type of PDF; G for Gaussian distribution, P for positively skewed ($Sk \approx 0.48$), and N for negatively skewed ($Sk \approx -0.48$).
- The second digit indicates the PS slope; 1 for $p = -1$ and 2 for $p = -2$.
- The following character(s) indicates the channel size; F for full channel ($8H \times 4H$), M for the minimal channel ($2.4H \times 0.8H$)

The roughness metrics that are widely used in roughness study are shown in Table 1. One of the full span roughness topographies $G2F$ is illustrated in figure 1. It is worth mentioning that the roughness for minimal channels and

full span channels are independently generated, which means each surface has an individual realization but the statistics are controlled by the generation method. By comparing each full span roughness with minimal span roughness, the stability of the generation method is demonstrated, nearly no discrepancy of the roughness statistics is exhibited. The grid size for DNS is mostly determined by the smallest in-plane roughness wavelength, $\lambda_1 = 0.08H$. In order to properly model each roughness elements with IBM, based on the mesh independent test approximately 8 computational cells are used for each roughness element, which lead to the simulation resolution $N_x \times N_y \times N_z = 900 \times 401 \times 480$ and $256 \times 401 \times 96$ for full span channel and minimal channel, respectively.

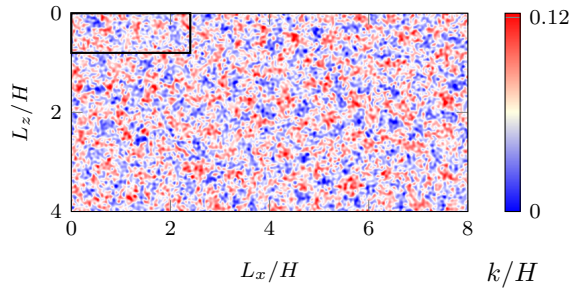


Figure 1: Full-span roughness sample $G2F$. The black rectangle represents the size of the minimal channel. Color bar shows the surface height.

3 Results

The DNS results, especially the mean velocity and temperature profiles, $\langle \bar{u} \rangle(y)$ and $\langle \bar{\theta} \rangle(y)$ are obtained by applying double-averaging:

$$\langle \bar{\Phi} \rangle(y) = \frac{1}{S} \iint_S \bar{\Phi}(x, y, z) dx dz . \quad (5)$$

Where $\bar{\Phi}(x, y, z)$ is the time averaged velocity \bar{u} /temperature $\bar{\theta}$ field. The angular bracket $\langle \cdot \rangle$ denotes horizontal averaging. The double-averaged velocity and temperature profiles will be denoted as U and Θ , respectively.

Furthermore, due to the fluctuating surface structure the origin of the wall normal coordinate of a rough surface cannot be naturally defined. In order to align the logarithmic layer of smooth and rough surfaces bounded velocity profile, zero plane displacement d is considered. To this end, Jackson (Jackson 1981) proposed use of moment centroid of the drag profile on rough surfaces as the virtual origin for the logarithmic velocity profile. The definition of the zero plane displacement d in present work follows Jackson's method. It is

Topography	Sk	p	k_{md}/H	k_{rms}/H	L_x^{corr}/H	S_f/S	ES	ΔU^+	$\Delta \Theta^+$
$P1F$	0.48	-1	0.046	0.0208	0.052	0.28	0.57	7.33	4.70
$P1M$	0.48	-1	0.046	0.0208	0.052	0.28	0.57	7.28	4.72
$P2F$	0.48	-2	0.046	0.0208	0.100	0.21	0.44	6.99	3.93
$P2M$	0.48	-2	0.046	0.0208	0.100	0.21	0.44	6.86	4.37
$G1F$	0	-1	0.061	0.0200	0.050	0.27	0.54	6.67	3.93
$G1M$	0	-1	0.061	0.0200	0.050	0.27	0.54	6.66	3.99
$G2F$	0	-2	0.061	0.0200	0.100	0.20	0.43	6.30	3.62
$G2M$	0	-2	0.061	0.0200	0.100	0.20	0.43	6.39	3.70
$N1F$	-0.48	-1	0.074	0.0208	0.052	0.28	0.57	6.14	4.73
$N1M$	-0.48	-1	0.074	0.0208	0.052	0.28	0.57	6.07	4.68
$N2F$	-0.48	-2	0.074	0.0208	0.100	0.21	0.44	5.82	4.44
$N2M$	-0.48	-2	0.074	0.0208	0.100	0.21	0.44	5.63	4.38

Table 1: Roughness topographical statistics, where S_f is the total frontal projected area of the roughness. L_x^{corr} refers to the length scale where the roughness auto-correlation in streamwise direction drops under 0.2. Simulation results are shown on the last two columns on the left.

also shown in the present work that d , derived from velocity field, also applies for temperature field.

Effect of channel size

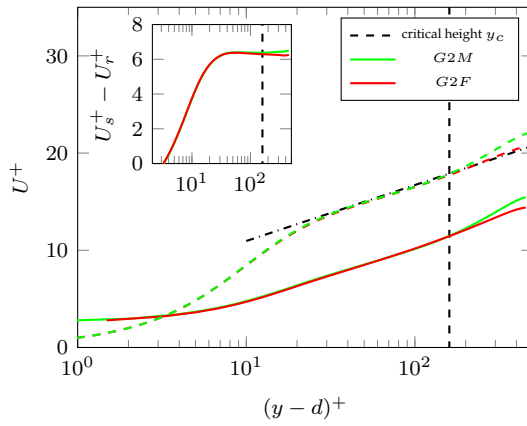


Figure 2: Mean velocity profile of roughness type $G2$, dashed line: velocity profile of smooth wall U_s^+ , solid line: velocity profile of rough wall U_r^+ . The inset shows the velocity retardation $U_s^+ - U_r^+$ as a function of wall normal distance $(y - d)^+$.

The velocity field of exemplary cases $G2M$ and $G2F$ are compared in figure 2. While the velocity offset profile is shown in the inset of figure 2 with identical coloring style. With the same measurement, temperature field predicted by minimal channel and full span channel is compared in figure 3. As one can observe, excellent agreement of the profiles are achieved between minimal channels and full span channels below each critical height y_c . Due to the nature of minimal channels, sudden increase of the profiles in outer layer can be observed for both smooth and rough cases. However, the offset profiles of minimal

channel and full span channel, as shown in the inset, collapse and reach constant values in logarithmic layer. The roughness function ΔU^+ as well as $\Delta \Theta^+$ are obtained by measuring the mean offset of the profile in logarithmic layer, specifically over $y^+ = 160 - 250$.

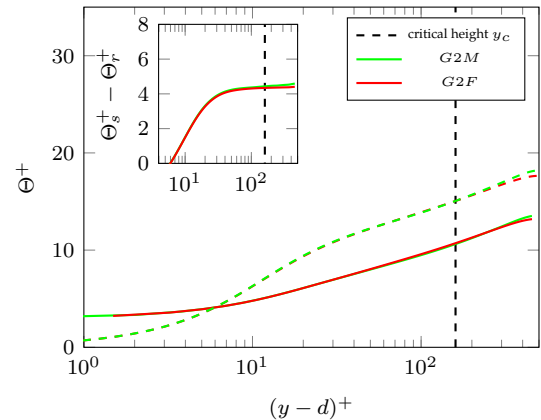


Figure 3: Mean temperature profile of roughness type $G2$, dashed line: temperature profile of smooth wall Θ_s^+ , solid line: temperature profile of rough wall Θ_r^+ . The inset shows the temperature retardation $\Theta_s^+ - \Theta_r^+$ as a function of wall normal distance $(y - d)^+$.

By generalizing the observation to all considered cases, ΔU^+ along with $\Delta \Theta^+$ are summarized on the last two columns in table 1. To visualize the disagreement of minimal channel with full span channel, graphical comparison are illustrated in figure 4. It can be observed that minimal channels show excellent agreement with the conventional full span channel, the disagreement of $\Delta U^+/\Delta \Theta^+$ lies under 5%. Consistent predictions indicate the capability of the minimal channels in reproducing the hydro- and thermody-

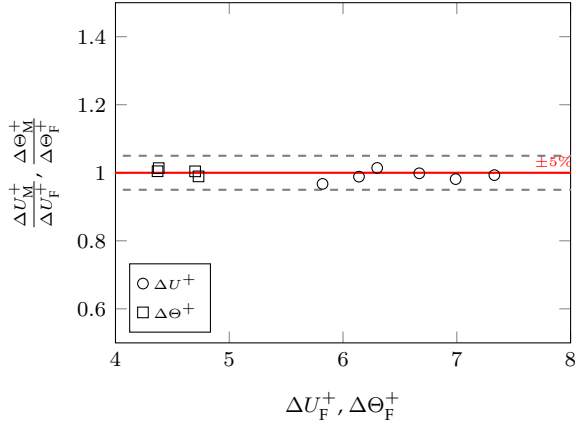


Figure 4: ΔU_M^+ and $\Delta \Theta_M^+$ predicted by minimal channels normalized by full span channel prediction ΔU_F^+ and $\Delta \Theta_F^+$, respectively \circ : ΔU^+ , \square : $\Delta \Theta^+$. Gray dashed lines indicate the boundary of 5% error interval around $\Delta U_M^+ / \Delta U_F^+ = \Delta \Theta_M^+ / \Delta \Theta_F^+ = 1$

namic properties of the irregular pseudo-realistic roughness. Furthermore, the consistent prediction results also imply the determining characters of roughness PS and PDF on both skin friction and heat transfer.

Effect of roughness topography

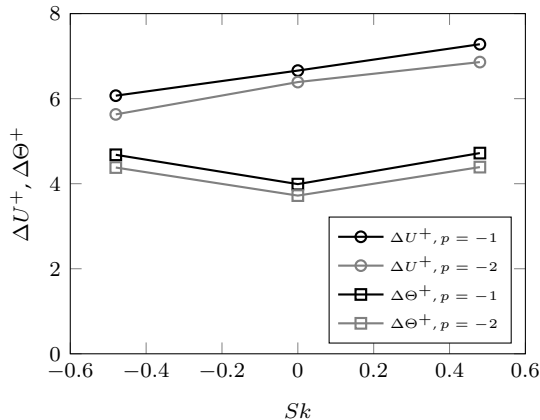


Figure 5: ΔU^+ (circles) and $\Delta \Theta^+$ (squares) predictions from minimal channels. Black: $p = -1$, gray: $p = -2$.

An overview of the roughness function ΔU^+ from minimal channel simulations is plotted in figure 5, where roughness function ΔU^+ is shown as a function skewness Sk , grouped by PS slope p . As investigated by Flack *et al.*(2020), positively skewed rough surfaces give higher skin friction than non-skewed or negatively skewed roughness. Negatively skewed surfaces show ‘slip-velocity’ effect (Jelly & Busse 2018), which translates into a weaker mean velocity retardation. The trend observed in the present results

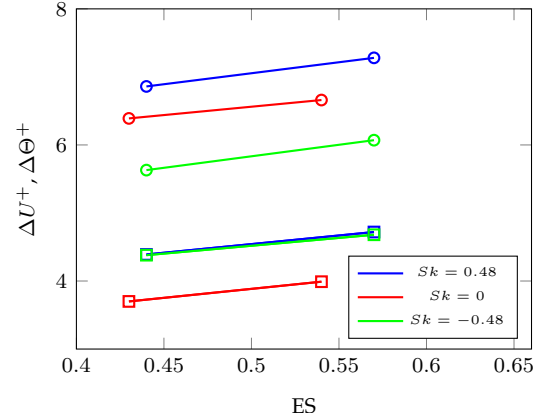


Figure 6: ΔU^+ (circles) and $\Delta \Theta^+$ (squares) predictions from minimal channels. Blue: $Sk = 0.48$, red: $Sk = 0$, green: $Sk = -0.48$.

fully agrees with what suggested by the previous researchers. On the other hand, less research are conducted to investigate the temperature field, the averaged offset of logarithmic temperature profile $\Delta \Theta^+$ analogous to ΔU^+ are integrated in figure 5. The evolution of $\Delta \Theta^+$ show significant difference to ΔU^+ . It is demonstrated that Gaussian surfaces show lowest interference to temperature field while these skewed roughness, regardless of its sign, can enhance the temperature offset. By adjusting the PS slope p an overall change of heat transfer ability of the roughness can be observed. To shed further light into the correlation of spatial roughness distribution and $\Delta \Theta^+$, $\Delta \Theta^+$ is plotted as a function of effective slope ES in figure 6. Approximately parallel increase of $\Delta \Theta^+$ with ES is exhibited. Similar trend can be found for ΔU^+ . The overlapping lines of $\Delta \Theta^+$ with $Sk = \pm 0.48$ illustrate that the peak dominant surfaces($Sk = 0.48$) show identical thermodynamic property to the pit dominant surfaces($Sk = -0.48$) given the same PS.

4 Conclusions

DNS is carried out for fully developed turbulent flow over artificial irregular roughness driven by constant pressure gradient. A source term for temperature field is applied while the temperature for the roughness is prescribed to be 0. The roughness topography is generated based on the random irregular roughness generation method proposed by Räfols & Almqvist(2019). Simulations are carried out at $Re_\tau \approx 500$. First of all, the stability of the roughness generation method is evaluated by showing the statistics of independently generated surfaces for full span channel and minimal channel. It is also demonstrated that the minimal channel is capable for reproducing the hydro- and thermodynamic proper-

ties of the artificial irregular roughness with considerable decrease of computational effort. In the present work, ΔU^+ and ΔT^+ are compared among the roughness topographies with systematically adjusted PDF and PS. 3 types of PDF, namely $Sk = 0, \pm 0.48$ are combined with 2 types of PS inputs whose $p = -1 \& -2$. It is found that the effect of roughness topography is different for skin friction and heat transfer. A monotonically increase of ΔU^+ as a function of Sk is observed, while for temperature field the skewed roughness, regard less peak or pit dominant, can enhance the heat transfer to an comparable extent. The effect of spatial distribution of the roughness, implied by PS slope p , show same trend to both velocity and temperature fields. This can be observed by the general and approximately parallel downward shift of ΔU^+ and $\Delta \Theta^+$ through varying ES.

Acknowledgments

Jiasheng Yang and Pourya Forooghi gratefully acknowledge financial support from Friedrich und Elisabeth Boysen-Foundation (BOY-151). This work was performed on the supercomputer ForHLR and the storage facility LSDF funded by the Ministry of Science, Research and the Arts Baden-Württemberg and by the Federal Ministry of Education and Research.

References

- Jiménez, J. (2004), Turbulent flows over rough walls, *Ann. Rev. Fluid Mech.* Vol. 36, pp. 173-196.
- Flack, K. A. (2018), Moving beyond Moody, *J. Fluid Mech.*, Vol. 842, pp. 1-4.
- Chung, D., Chan, L., MacDonald, L., Hutchins, N. and Ooi, A. (2015), A fast direct numerical simulation method for characterising hydraulic roughness, *J. Fluid Mech.*, Vol. 773, pp. 418-431.
- Pérez-Ràfols, F. and Almqvist, A. (2019), Generating randomly rough surfaces with given height probability distribution and power spectrum, *Tribology International*, Vol. 131, pp. 591-604.
- Flack, K. A. and Schultz, M. P. (2010), Review of Hydraulic Roughness Scales in the Fully Rough Regime, *J. Fluids Engineering*, Vol. 132.
- Napoli, E., Armenio, V. and De Marchis, M (2008). The effect of the slope of irregularly distributed roughness elements on turbulent wall-bounded flows, *J. Fluid Mech.*, Vol. 613. pp. 385-394.
- MacDonald, M., Chung, D. Hutchins, N., Chan, L., Ooi, A. and García-Mayoral, A. (2016), The minimal channel: a fast and direct method for characterising roughness, *Journal of Physics: Conference Series*, Vol. 708,
- Sigal, A., Danberg, J. E. (2008), New correlation of roughness density effect on the turbulent boundary layer, *AIAA Journal*, Vol. 28, pp. 554-556.
- Goldstein, D., Handler, R. and Sirovich, L., Modeling a no-slip flow boundary with an external force field., *Journal of Computational Physics*, Vol. 105, pp. 354-366.
- Forooghi, P., Flory, M., Bertsche, D., Wetzel, T. and Frohnapfel, B. (2017a). Heat transfer enhancement on the liquid side of an industrially designed flat-tube heat exchanger with passive inserts-numerical investigation. *Appl. Therm. Eng.*, Vol. 123, pp. 573-583.
- Bons, J.P. (2005) A critical assessment of Reynolds analogy for turbine flows. *ASME J. Heat Transf.*, Vol. 127(5), pp. 472-485.
- Kader, B. A. (1981) Temperature and concentration profiles in fully turbulent boundary layers. *Intl. J. Heat Mass Transfer*, Vol. 24, pp. 1541-1544.
- Cebeci, T. and Bradshaw, P. (1984), Physical and computational aspects of convective heat transfer. Springer.
- MacDonald, M., Hutchins, N., Chung, D. (2019), Roughness effects in turbulent forced convection, *J. Fluid Mech.*, Vol. 861, pp. 138-162.
- Barros, J. M., Schultz, M. P. and Flack, K. A. (2018), Measurements of skin-friction of systematically generated surfaces roughness, *International Journal of Heat and Fluid Flow*, Vol. 72, pp. 1-7.
- Nikora, V. I., Stoesser, T., Cameron, S. M., Stewart, M., Papadopoulos, K., Ouro, P., McSherry, R., Zampiron, A., Marusic, I., Falconer, R. A. and et al (2019), Friction factor decomposition for rough-wall flows: theoretical background and application to open-channel flows, *Journal of Fluid Mechanics*, Vol. 872, pp. 626-664.
- Flack, K.A., Schultz, M.P. & Barros, J.M. 2020 Skin friction measurements systematically-varied roughness: Probing the role of roughness amplitude and skewness. *Flow, Turbulence and Combustion*, Vol. 104, pp.317-329.
- Jelly, T.O. & Busse, A. 2018 Reynolds and dispersive shear stress contributions above highly skewed roughness *Journal of Fluid Mechanics* vol. 852, pp. 710-724.
- Jackson, P.S. 1981 On the displacement height in the logarithmic velocity profile. *Journal of Fluid Mechanics* vol.111, pp.15-25.